Non-Interpenetrated Metal-Organic Frameworks Based on Copper(II) Paddlewheel and Oligoparaxylene-Isophthalate Linkers: Synthesis, Structure and Gas Adsorption

Yong Yan,[1,2†] Michal Juríček,[3,4†] François-Xavier Coudert,[5] Nicolaas A. Vermeulen,[3] Sergio Grunder,[3] Anne Dailly,[6] William Lewis,[1] Alexander. J. Blake,[1] J. Fraser Stoddart[3*] and Martin Schröder[1,2*]

1. *School of Chemistry, University of Nottingham, University Park, Nottingham, NG7 2RD, UK.*

2. *School of Chemistry, Oxford Road, University of Manchester, Manchester, M13 9PL, UK.*

3. *Center for the Chemistry of Integrated Systems, Department of Chemistry, Northwestern University, 2145 Sheridan Road, Evanston, Illinois 60208, United States.*

4. *Department of Chemistry, University of Basel, St. Johanns-Ring 19, 4056 Basel, Switzerland.*

5. *PSL Research University, Chimie ParisTech-CNRS, Institut de Recherche de Chimie Paris, 75005 Paris, France.*

6. *Chemical and Environmental Sciences Laboratory, General Motors Corporation, Warren, Michigan 48090, United States.*

Email: M.Schroder@manchester.ac.uk; stoddart@northwestern.edu

[†]These authors contributed equally to this work.

Keywords: metal-organic framework, Shear modulus, copper, methane, hydrogen, hydrocarbon, gas storage

Abstract:

Two ~~{$Cu_2(COO)_4$} paddlewheel~~ metal-organic framework materials, MFM-130 and MFM-131~~,~~ (MFM = Manchester Framework Material, previously designated NOTT) have been ~~synthesised~~ synthesized using two oligoparaxylene (OPX) tetracarboxylate linkers containing four and five aromatic rings, respectively. Both **fof**-type non-interpenetrated networks contain Kagomé lattice layers comprising {$Cu_2(COO)_4$} paddlewheel units and isophthalates, which are pillared by the OPX linkers. Desolvated MFM-130, MFM-130a, ~~shows~~ with permanent porosity ~~(with a~~ BET surface area of 2173 m^2/g, ~~and~~ pore volume of 1.0 cm^3/g)~~.~~ ~~MFM-130a~~ reveals high H_2 storage capacity at 77 K of 5.3 wt% at 20 bar and 2.2 wt% at 1 bar, and a higher CH_4 adsorption uptake of 163 cm^3(STP)/cm^3 (35 bar and 298 K) compared with its structural analogue NOTT-103.~~.~~ ~~Compared to its structural analogue, NOTT-103, which incorporates the analogous oligophenylene linker, MFM-130a shows a higher CH_4 adsorption capacity of 163 cm^3(STP)/cm^3 at 35 bar, as well as a higher working capacity at 298 K for CH_4 of 130 cm^3/cm^3 between 5 and 65 bar. Because of the presence of open Cu(II) sites and methyl substituents, MFM-130a exhibits high CO_2 adsorption capacity and high selectivities for CO_2 vs N_2 and CO_2 vs CH_4 at room temperature based upon comparisons of Henry's Law constants for these substrates~~. MFM-130a also reveals impressive selective adsorption of C_2H_2, C_2H_4 and C_2H_6 over CH_4 at room temperature, indicating its potential ~~that MFM-130a is a promising microporous material~~ for separation of C_2 hydrocarbons from CH_4. The single crystal structure of MFM-131~~,~~ ~~incorporating OPX linkers with five aromatic rings,~~ confirms that the methyl substituents of the paraxylene units block the windows in the Kagomé lattice layer of the framework. This effectively inhibits network interpenetration in MFM-131, ~~which, therefore, has a non-interpenetrated structure.~~ ~~This~~ which contrasts with its doubly-interpenetrated oligophenylene analogue~~,~~ NOTT-104~~, which is doubly-interpenetrated in the solid-state~~. A calculation study on the mechanical properties of these two MOFs confirms and explains the instability of MFM-131 upon desolvation in contrast to the behavior of MFM-130. The incorporation of paraxylene units, therefore, provides an efficient method for preventing network interpenetration as well as accessing new functional materials with modified and selective sorption properties for gas substrates.

Introduction

Nanoporous metal–organic frameworks (MOFs) constructed from metal cations and clusters bridged by polyfunctional organic linkers are an important class of hybrid materials which show great promise for gas-storage and separation applications.[1] An advantage of porous MOFs is that their design, structure and properties can be varied by modification of the organic linkers which can have different lengths, topologies, and geometries and can incorporate functional groups to enhance preferential binding of guest substrates *via* optimised pore shapes/diameters for molecular separation.[2] We have developed[3] a series of framework materials employing linear tetracarboxylate linkers and $\{Cu_2(COO)_4\}$ paddlewheel units[3] to generate **fof**-type[4] networks.[4] The assembly of isophthalate (benzene-3,5-dicarboxylate) units within tetracarboxylate linkers with $\{Cu_2(COO)_4\}$ paddlewheels generates two-dimensional Kagomé lattices, which are pillared by the aromatic backbones of these linkers. Two types of cage structures are formed within this assembly: Cage A, an ellipsoid-shaped cage formed by six linkers and two triangular $\{(Cu_2)_3(isophthalate)_3\}$ windows at the two ends, with a larger hexagonal $\{(Cu_2)_6(isophthalate)_6\}$ core structure, and Cage B, a more cylindrical cage formed also by six linkers and two triangular $\{(Cu_2)_3(isophthalate)_3\}$ windows. These materials show high porosity and high H_2 and CH_4 storage capacity, with the porosity, storage capacity and binding energies with H_2 and CH_4 being tuned by modification of the organic linkers.[3] Elongation of the linear tetracarboxylate units can increase the porosity of the resultant structures,[3b] but network interpenetration in these **fof**-systems can occur when the linker is lengthened beyond a certain point. Thus, development of highly porous and non-interpenetrated structures in these systems remains a challenge.[5] There are several strategies for building non-interpenetrated networks with large organic linkers: (i) building networks with intrinsically non-interpenetrating topologies such as **rht**[6] and **flu**[7], (ii) optimising the synthesis of MOF materials using different solvents, conditions and template effects to target preferred non-interpenetrating networks,[8] and (iii) introducing bulky functional groups in the organic units to create steric hindrance.[9]

Oligoparaxylenes (OPXs) have been developed as efficient building blocks for the construction of MOFs with Zn(II)/Mg(II) nodes.[10,11] The methyl substituents present in OPXs increase dramatically the solubility of longer oligomers compared to oligophenylene analogues, which become increasingly less soluble with increasing length over just a few aromatic rings. OPX linkers can thus serve as stable, extended and, most importantly, soluble organic building units or struts. A series of non-interpenetrating MOF-74 analogues

have been successfully constructed from 4-carboxylate OPX tectons to give a series of isorecticular Mg(II) frameworks with pore apertures ranging from 1.4 to 9.8 nm.[11] We reasoned that the synthesis of non-interpenetrating **fof**-type networks structures might be achieved using OPX units serving as linear aromatic backbones to connect two isophthalate units to form extended, yet soluble, tetracarboxylate linkers. We envisaged that frameworks with optimized pore size, geometry and functionality could be accessed by employing such OPX-derived linkers rather than using the more problematic, insoluble oligophenylene units. It is worth noting that methyl substituents present in the OPX struts can not only create hydrophobic pockets,[3e] which can aid gas adsorption and separation, but can also impart a degree of steric bulk within pores.

We report herein the synthesis of two new OPX-based linkers, the tetracarboxylates $\mathbf{H_4L^{IV}}$ and $\mathbf{H_4L^{V}}$ (Figure 1) incorporating isophthalate moieties, and their coordination to $\{Cu_2(COO)_4\}$ paddlewheel nodes to form the non-interpenetrated **fof**-type frameworks MFM-130 and MFM-131. MFM-131 is the first example of a **fof**-type MOF with ultra-long organic struts that does not show network interpenetration. The H_2, CH_4, CO_2 and small hydrocarbons adsorption in the desolvated form of MFM-130, MFM-130a, has been investigated, and the selective adsorption of CO_2 over N_2, and C_2 hydrocarbons (acetylene, ethylene and ethane) over CH_4 in this material are discussed. Desolvation of MFM-131, however, leads to collapse of this material and loss of porosity. A calculation study on the mechanical properties of these two MOFs in the elastic regime was, therefore, performed to confirm and explain their distinct properties upon desolvation.

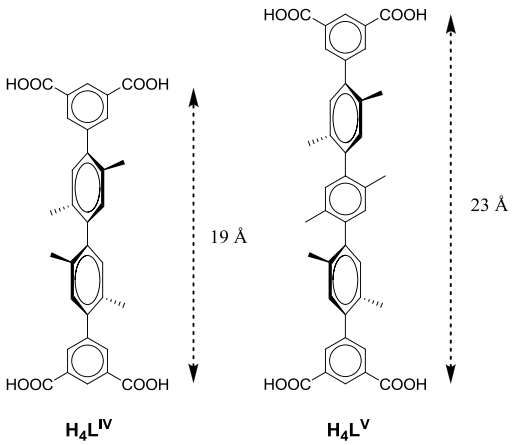

Figure 1. View of two OPX-based tetracarboxylate linkers $\mathbf{H_4L^{IV}}$ and $\mathbf{H_4L^{V}}$.

Experimental Section

Materials and Instrumentation. All reagents were purchased from commercial suppliers and used without further purification unless stated otherwise. 4,4'-Diiodo-2,2',5,5'-tetramethyl-1,1'-biphenyl[12] was synthesised as previously reported.[12] Thin-layer chromatography (TLC) was performed on Merck™ TLC plates (F254 indicator), and column chromatography carried out on Merck™ silica gel 60 (Merck Grade 9385, 0.040–0.063 mm). Nuclear magnetic resonance (NMR) spectra were recorded on a BrukerAvance III 500 MHz NMR spectrometer at working frequencies of 499.842 (^{1}H) and 125.579 (^{13}C) MHz. The signal corresponding to the residual non-deuterated solvent ($CDCl_3$: δ_H = 7.26 ppm and δ_C = 77.16 ppm; DMSO-d_6: δ_H = 2.50 ppm and δ_C = 39.52 ppm; PhMe-d_8: δ_H = 2.08 ppm and δ_C = 20.43 ppm) was used as a reference. Solutions of **1** and **4** in PhMe-d_8 were pre-heated at 90 °C for 30 min before acquiring their ^{1}H and ^{13}C NMR spectra at 25 °C. High-resolution mass spectra (HRMS) were measured on an Agilent 6210 Time-of-Flight (ToF) LC-MS using an ESI source coupled with Agilent 1100 HPLC stack *via* direct infusion (0.6 mL/min). Fourier transform infrared (FTIR) spectra were performed on a Nicolet iS5 spectrophotometer using the attenuated total reflectance (ATR) mode. Elemental analyses were carried out on a CE-440 elemental analyser, and thermalgravimetric analyses (TGA) were performed using a TA SDT-600 thermogravimetric analyser under a flow of N_2 (20 mL/min) with a heating rate of 5 °C/min. Powder X-ray diffraction (PXRD) measurements were carried out at room temperature on a PANalytical X'Pert PRO diffractometer with CuKα_1 radiation (λ = 1.5406 Å) at 40 kV, 40 mA with a scan speed of 0.02°/s and a step size of 0.005° in 2θ (Figure S2).

Gas Sorption Measurements. H_2, CO_2 and N_2 isotherms were collected using an IGA gravimetric adsorption apparatus (Hiden) in a clean ultra-high-vacuum system with a diaphragm and turbo pumping system. Approximately 120 mg of solvent-exchanged sample was loaded into the sample basket within the adsorption instrument and then degassed under dynamic vacuum at 110 °C for 12 h to obtain the fully desolvated sample. In H_2 adsorption experiments, ultra-pure plus grade H_2 (99.9995%, BOC Gases) was purified further using calcium aluminosilicate and activated carbon adsorbents to remove trace amounts of water and other impurities before introduction into the IGA system. Volumetric CH_4 sorption measurements were performed over the pressure range 0−70 bar using an automatically controlled Sievert's apparatus (PCT-Pro 2000 from Hy-Energy LLC). Low-pressure (< 1 bar) adsorption measurements for C_2 hydrocarbons were performed using an Autosorb 1-MP instrument (Quantachrome Instruments). Ultra-high-purity grade C_2H_2, C_2H_4 and C_2H_6 were used for adsorption measurements.

The temperature-dependent adsorption data were analyzed using the Virial equation:[13]

$$\ln\left(\frac{n}{p}\right) = A_0 + A_1 n + A_2 n^2 + \cdots$$

where the p is pressure, n is the amount adsorbed and A_0, A_1, *etc*. are Virial coefficients. The Henry's Law constant (K_H) is equal to exp(A_0), and the selectivity can be derived from the ratio of the constants K_H for different gases.

Synthesis of H_4L^{IV}.

2',2'',5',5''-Tetramethyl-[1,1':4',1'':4'',1'''-quaterphenyl]-3,3''',5,5'''-tetracarboxylate tetramethyl ester (1). A mixture of 5-(4,4,5,5-tetramethyl-1,3,2-dioxaborolan-2-yl)benzene-1,3-dicarboxylate dimethyl ester (1.66 g, 5.17 mmol), 4,4'-diiodo-2,2',5,5'-tetramethyl-1,1'-biphenyl (1.09 g, 2.35 mmol), $PdCl_2$(dppf)•CH_2Cl_2 (0.20 g, 0.24 mmol), CsF (2.14 g, 14.1 mmol), *p*-dioxane (10 mL) and H_2O (5 mL) was heated at reflux for 18 h under Ar before H_2O (50 mL) was added. The reaction mixture was extracted twice with CH_2Cl_2 and the combined organic extracts were washed with brine and dried over $MgSO_4$. After filtration, the solvent was removed by evaporation and the residue purified by column chromatography over silica gel using hexane/CH_2Cl_2 (1:1 to 0:1) as eluent to afford the pure product (1.16 g, 83%) as a white solid and as a mixture of two enantiomers (*R* and *S*), undergoing fast racemization at room temperature. ^{1}H NMR (500 MHz, PhMe-d_8, ppm): δ 8.94 (t, J = 1.6 Hz, 2H), 8.41 (d, J = 1.6 Hz, 4H), 7.11 (s, 2H), 7.04 (s, 2H), 3.52 (s, 12H), 2.16 (s, 6H), 2.06 (s, 6H). ^{13}C NMR (125 MHz, PhMe-d_8, ppm): δ (one signal could not be detected because of the signal overlap) 165.8, 143.1, 141.6, 139.3, 134.7, 133.9, 132.7, 131.9, 131.6, 131.3, 51.8, 19.9, 19.4. HRMS (ESI): *m/z* calcd for $C_{36}H_{34}O_8$: 595.2326 ([M + H]$^+$); found 595.2330.

2',2'',5',5''-Tetramethyl-[1,1':4',1'':4'',1'''-quaterphenyl]-3,3''',5,5'''-tetracarboxylic acid (H_4L^{IV}). A mixture of **1** (1.12 g, 1.88 mmol), aq. NaOH (0.5 M, 30 mL) and THF (30 mL) was heated at 50 °C for 21 h. THF was then removed by evaporation and concentrated HCl added (pH ~ 1) to the aqueous residue. The precipitate thus formed was collected by filtration, washed with H_2O, and dried in air to afford the product (975 mg, 97%) as a white solid and as a mixture of two enantiomers (*R* and *S*) undergoing fast racemization at room temperature. ^{1}H NMR (500 MHz, DMSO-d_6, ppm): δ 13.48 (br, 4H), 8.48 (t, J = 1.6 Hz, 2H), 8.14 (d, J = 1.5 Hz, 4H), 7.25 (s, 2H), 7.11 (s, 2H), 2.24 (s, 6H), 2.09 (s, 6H). ^{13}C NMR (125 MHz, DMSO-d_6,

ppm): δ 166.6, 141.8, 140.5, 138.3, 133.7, 133.3, 131.9, 131.6, 131.4, 131.0, 128.5, 19.6, 19.1. HRMS (ESI): *m/z* calcd for $C_{32}H_{26}O_8$: 537.1555 ([*M* – H]$^-$); found 537.1544.

Synthesis of H_4L^V.

4'-Bromo-2',5'-dimethyl-[1,1'-biphenyl]-3,5-dicarboxylate dimethyl ester (2). A mixture of 5-(4,4,5,5-tetramethyl-1,3,2-dioxaborolan-2-yl)benzene-1,3-dicarboxylate dimethyl ester (3.56 g, 11.1 mmol), 1,4-dibromo-2,5-dimethyl-benzene (14.6 g, 55.5mmol), $PdCl_2$(dppf)•CH_2Cl_2 (0.46 g, 0.56 mmol), CsF (5.06 g, 33.3 mmol), *p*-dioxane (40 mL) and H_2O (20 mL) was heated at reflux under Ar for 18 h before H_2O (100 mL) was added. The reaction mixture was extracted twice with CH_2Cl_2 and the combined organic extracts were washed with brine and dried over $MgSO_4$. After filtration, the solvent was removed by evaporation and the residue purified by column chromatography over silica gel using hexane/CH_2Cl_2 (9:1 to 0:1) as the eluent to afford the pure product (5.98 g, 71%) as a white solid. ^{1}H NMR (500 MHz, $CDCl_3$, ppm): δ 8.67 (t, *J* = 1.6 Hz, 1H), 8.16 (d, *J* = 1.7 Hz, 2H), 7.47 (s, 1H), 7.09 (s, 1H), 3.96 (s, 6H), 2.39 (s, 3H), 2.19 (s, 3H). ^{13}C NMR (125 MHz, $CDCl_3$, ppm): δ 166.3, 141.8, 139.0, 135.6, 134.6, 134.4, 134.1, 132.0, 130.8, 129.5, 124.6, 52.7, 22.4, 19.7. HRMS (ESI): *m/z* calcd for $C_{18}H_{17}BrO_4$: 377.0383 ([*M* + H]$^+$); found 377.0392.

2',5'-Dimethyl-4'-(4,4,5,5-tetramethyl-1,3,2-dioxaborolan-2-yl)-[1,1'-biphenyl]-3,5-dicarboxylate dimethyl ester (3). A mixture of **2** (5.71 g, 15.1 mmol), bis(pinacolato)diboron (4.22 g, 16.6 mmol), $PdCl_2$(dppf)•CH_2Cl_2 (0.62 g, 0.76 mmol), KOAc (4.46 g, 45.4 mmol) and dry DMSO (60 mL) was heated at 80 °C under Ar for 24 h before H_2O (400 mL) was added. The precipitate thus formed was collected by filtration and washed with twice with H_2O (~1 L in total) before it was dissolved in CH_2Cl_2 and the organic solution dried over $MgSO_4$. After filtration, the solvent was removed by evaporation and the residue purified by column chromatography over silica gel using hexane/CH_2Cl_2 (1:1 to 0:1) as eluent to afford the pure product (5.20 g, 87%) as a white solid. ^{1}H NMR (500 MHz, $CDCl_3$, ppm): δ 8.66 (t, *J* = 1.7 Hz, 1H), 8.19 (d, *J* = 1.6 Hz, 2H), 7.69 (s, 1H), 7.05 (s, 1H), 3.96 (s, 6H), 2.54 (s, 3H), 2.22 (s, 3H), 1.37 (s, 12H). ^{13}C NMR (125 MHz, $CDCl_3$, ppm): δ (one signal could not be detected because of the signal overlap) 166.4, 142.8, 142.7, 142.1, 138.2, 134.4, 131.4, 131.2, 130.6, 129.2, 83.6, 52.6, 25.0, 21.8, 19.7. HRMS (ESI): *m/z* calcd for $C_{24}H_{29}BO_6$: 425.2134 ([*M* + H]$^+$); found 425.2140.

2',2'',2''',5',5'',5'''-Hexamethyl-[1,1':4',1'':4'',1''':4''',1''''-quinquephenyl]-3,3'''',5,5''''-tetra carboxylate tetramethyl ester (4). A mixture of **3** (1.67 g, 4.21 mmol), 1,4-diiodo-2,5-dimethylbenzene (0.726 g, 2.00mmol), $PdCl_2$(dppf)•CH_2Cl_2 (0.16 g, 0.20 mmol), CsF (1.82 g, 12.0 mmol), *p*-dioxane (8 mL)

and H_2O (4 mL) was heated at reflux under Ar for 38 h before it was cooled to room temperature, and the solid collected by filtration and washed with H_2O. The solid residue was purified by column chromatography over silica gel using CH_2Cl_2, CH_2Cl_2/PhMe (2:1 to 1:1) and PhMe/ethyl acetate (99.5:0.5 to 95:5) as eluents to afford the product (759 mg, 54%) as a white solid and as a ~1:1 mixture of two diastereoisomers, a pair of enantiomers (*RR* and *SS*), and one *meso* isomer (*RS*) undergoing fast isomerization at room temperature. ^{1}H NMR (500 MHz, PhMe-d_8, ppm): δ 8.96–8.94 (m, two partially overlapped triplets, J = 1.5 Hz, 2H), 8.42–8.41 (m, two partially overlapped doublets, J = 1.5 Hz, 4H), 7.16–7.14 (m, two partially overlapped singlets, 2H), 7.12–7.10 (m, two partially overlapped singlets, 2H), 7.06–7.03 (m, two almost resolved singlets (~1:1 ratio), 2H), 3.51 (m, two overlapped singlets, 12H), 2.17–2.15 (m, two partially overlapped singlets, 6H), 2.15–2.12 (m, two almost resolved singlets (~1:1 ratio), 6H), 2.10–2.06 (m, two resolved singlets (~1:1 ratio), 6H). ^{13}C NMR (125 MHz, PhMe-d_8, ppm): δ (six signals could not be detected because of the signal overlap) 165.83, 165.82, 143.1, 142.0, 141.9, 140.83, 140.80, 139.22, 139.21, 134.8, 134.0, 133.9, 133.3, 132.7, 132.6, 132.11, 132.06, 131.6, 131.31, 131.25, 131.2, 129.5, 51.80, 51.79, 19.91, 19.90, 19.64, 19.62, 19.44, 19.42. HRMS (ESI): *m/z* calcd for $C_{44}H_{42}O_8$: 699.2952 ([M + H]$^+$); found 699.2959.

2',2'',2''',5',5'',5'''-Hexamethyl-[1,1':4',1'':4'',1''':4''',1'''':4'''',1''''-quinquephenyl]-3,3'''',5,5''''-tetracarboxylic acid (H_4L^V). A mixture of **4** (735 mg, 1.05mmol), aq. NaOH (0.5 M, 30 mL) and THF (30 mL) was heated at 50 °C for 42 h. The THF was removed by evaporation and concentrated HCl added to the aqueous residue to pH ~ 1. The precipitate thus formed was collected by filtration, washed with H_2O and dried in air to afford the pure product (705 mg, 98%) as a white solid and as a ~1:1 mixture of two diastereoisomers, a pair of enantiomers (*RR* and *SS*), and one *meso* isomer (*RS*) undergoing fast isomerization at room temperature. ^{1}H NMR (500 MHz, DMSO-d_6, ppm): δ 13.40 (m, two overlapped broad singlets, 4H), 8.51–8.46 (m, two overlapped triplets, J = 1.7 Hz, 2H), 8.17–8.12 (m, two overlapped doublets, J = 1.7 Hz, 4H), 7.27–7.06 (m, six almost resolved singlets, 6H), 2.29–2.20 (m, two overlapped singlets, 6H), 2.13–2.08 (m, two overlapped singlets, 6H), 2.08–2.03 (m, two partially resolved singlets (~1:1 ratio), 6H). ^{13}C NMR (125 MHz, DMSO-d_6, ppm): δ (eleven signals could not be detected because of the signal overlap) 166.6, 141.9, 140.82, 140.79, 139.6, 138.2, 133.7, 133.27, 133.26, 132.39, 132.38, 131.9, 131.8, 131.5, 130.9, 130.50, 130.46, 128.5, 19.54, 19.45, 19.2, 19.1, 18.9. HRMS (ESI): *m/z* calcd for $C_{40}H_{34}O_8$: 641.2181 ([M – H]$^-$); found 641.2177.

Synthesis of $[Cu_2(L^{IV})(H_2O)_2]$•6DMF•3H_2O (MFM-130). H_4L^{IV} (50 mg, 0.093 mmol) and $Cu(NO_3)_2$•2.5H_2O (172.7 mg, 0.72 mmol) were dissolved in a mixture of N,N'-dimethylformamide (DMF, 6.0 mL) and H_2O (0.5 mL) and the solution placed in a pressure tube (15 mL). Upon addition of 6 M HCl (15 μL), the tube was capped and heated at 90 °C for 16 h, and a large amount of microcrystalline product precipitated. The blue crystals were collected by filtration and washed with warm DMF and dried in air. Yield: 58.6 mg (80%). Selected FTIR (cm^{-1}): 3404 (br, w), 2927 (w), 1657 (vs), 1626 (s), 1588 (m), 1494 (m), 1435 (m), 1417 (m), 1367 (vs), 1308 (w), 1284 (w), 1254 (m), 1187 (w), 1149 (w), 1094 (s), 1062 (m), 923 (w), 888 (w), 778 (m), 727 (s), 701 (w), 686 (w), 660 (s), 632 (w). Anal. Calcd (%) for $C_{50}H_{74}Cu_2N_6O_{19}$: C, 50.46; H, 6.27; N, 7.06. Found (%): C, 50.38; H, 5.75; N, 7.70.

Synthesis of $[Cu_2(L^{V})(H_2O)_2]$•7DMF•4H_2O (MFM-131). H_4L^{V} (50 mg, 0.078 mmol) and $Cu(NO_3)_2$•2.5H_2O (144.7 mg, 0.622 mmol) were dissolved in a mixture of DMF(7.0 mL) and H_2O (1.0 mL) in a pressure tube (15 mL). Upon addition of 6 M HCl (20 μL), the tube was capped and heated in an oil bath at 85 ^oC for 48 h to afford blue crystals. The reaction mixture was allowed to cool to room temperature, and the crystals were washed with warm DMF and dried in air. Yield: 60.9 mg, 85% based on H_4L^{V}. FT-IR (cm^{-1}): 3399 (br, w), 2924 (w), 1656 (vs), 1625 (s), 1589 (m), 1489 (m), 1435 (w), 1417 (w), 1367 (vs), 1303 (w), 1254 (m), 1186 (w), 1094 (s), 1062 (m), 955 (w), 887 (m), 777 (s), 736 (m), 724 (s), 700 (w), 660 (s). Anal. Calcd (%) for $C_{61}H_{91}Cu_2N_7O_{21}$: C, 52.88; H, 6.62; N, 7.08. Found (%): C, 52.48; H, 5.88; N, 7.45.

X-ray Crystallographic Analyses. Single-crystal diffraction data for MFM-130 were collected at 150(2) K on a Bruker SMART APEX CCD area detector using graphite monochromated Mo-Kα radiation. Data for MFM-131 were collected at beamline I19 at Diamond Synchrotron Light Source. The details for data collection are included in the CIF files in the Supporting Information. The structures were solved by the direct method and refined by full-matrix least-squares methods on F^2 using the SHELX-2013 program package.[14] Hydrogen atoms on the ligands were placed geometrically and refined using a riding model, and the hydrogen atoms of the coordinated water molecules could not be located but are included in the formula. "DFIX", "SADI", and "PART" commands were used to deal with the disorder of the paraxylene moieties in the structures. The SQUEEZE option of PLATON[15] was used to eliminate the contribution of disordered guest molecules to the reflection intensities.

Results and Discussion

Single Crystal X-Ray Structures. The tetracarboxylate ligands $\mathbf{H_4L^{IV}}$ and $\mathbf{H_4L^{V}}$ (Figure 1) were synthesised (Scheme 1) by a series of Suzuki cross-coupling reactions followed by hydrolysis of the resultant tetraesters. The synthetic procedures and characterization of the target compounds and all their precursors are provided in full detail in the Experimental Section. Based on the lengths of these two linear struts (approximately 19 Å for $\mathbf{H_4L^{IV}}$and 23 Å for $\mathbf{H_4L^{V}}$ based on distance between the two 4-C carbon atoms of the terminal isophthalate units), it was anticipated that nanosized porous structures can be assembled.

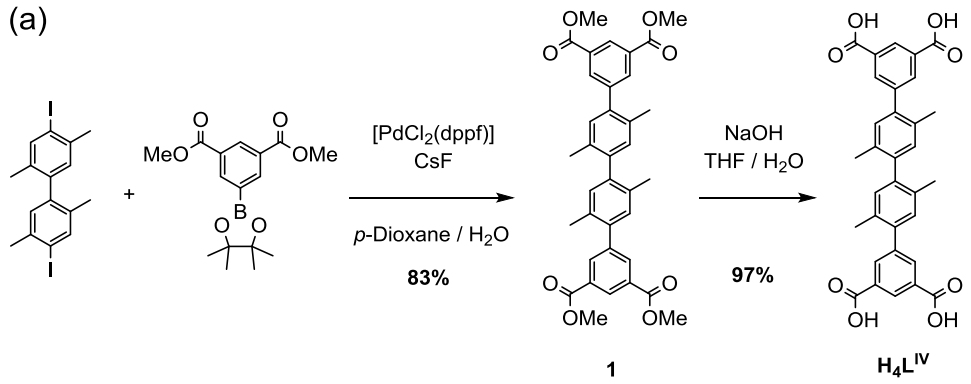

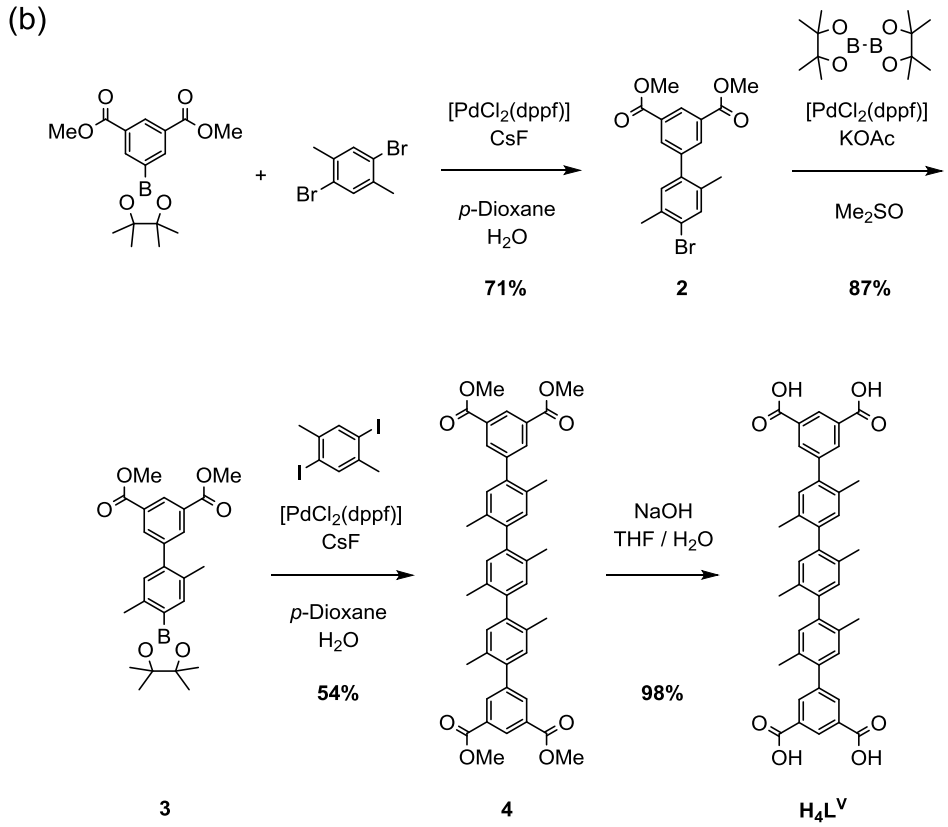

Scheme 1. Synthesis of $\mathbf{H_4L^{IV}}$ and $\mathbf{H_4L^{V}}$

Solvothermal reactions of $\mathbf{H_4L^{IV}}$ and $\mathbf{H_4L^{V}}$ with $Cu(NO_3)_2 \bullet 2.5H_2O$ in a mixture of DMF and H_2O at 80 °C for 16 h afforded blue highly crystalline solids of $[Cu_2(\mathbf{L^{IV}})(H_2O)_2] \bullet 6DMF \bullet 3H_2O$ (MFM-130) and $[Cu_2(\mathbf{L^{V}})(H_2O)_2] \bullet 7DMF \bullet 4H_2O$ (MFM-131), respectively. The formula of these two compounds were confirmed by elemental analysis, single crystal X-ray structure determinations, and by thermal gravimetric analysis (TGA) (Figure S1). The phase purity of the two bulk crystalline solids was confirmed by powder X-ray diffraction and Le Bail analyses (~~PXRD,~~ Figure S2–S4). Single-crystal X-ray structure analysis revealed that both MFM-130 and MFM-131 crystallise in *R*-3 space group. Both rhombohedral lattices in MFM-130 and MFM-131 have similar *a*-axes due to the same type of Kagomé lattice formed by the 2-connected isophthalate units with 4-connected $\{Cu_2(COO)_4\}$ paddlewheels. In MFM-130 (Figure 2), because of the steric hindrance caused by methyl substituents, the two connected paraxylene units in $(\mathbf{L^{IV}})^{4-}$ are almost perpendicular with respect to each other. The methyl group of the paraxylene unit adjacent to the isophthalate ring forces these two rings to be non-coplanar with a torsion angle of approximately 51°. Thus, the geometrical conformation of the central pair of paraxylene units "lock" the two terminal isophthalate moieties within the same plane, making the linker $(\mathbf{L^{IV}})^{4-}$ a planar 4-connected node when bound to $\{Cu_2\}$ paddlewheels. MFM-130 has an **fof**-type network topology constructed by the packing of two types of cages (A and B), and is isostructural with the analogous NOTT-102 constructed from tetracarboxylate linkers containing phenylene instead of paraxylene units.[3b] With the methyl groups ~~projected~~ projecting into the pores, both Cage A and Cage B in MFM-130 have reduced accessible voids compared to those of the non-functionalised analogue NOTT-102. Cage A has a slim ellipsoid shape with a length of 33 Å, a narrow diameter of 7 Å at the two ends and a larger diameter of 18 Å in the centre, while Cage B has a thicker cylinder shape with diameter of 13 Å and length of 16 Å (Figure 2).

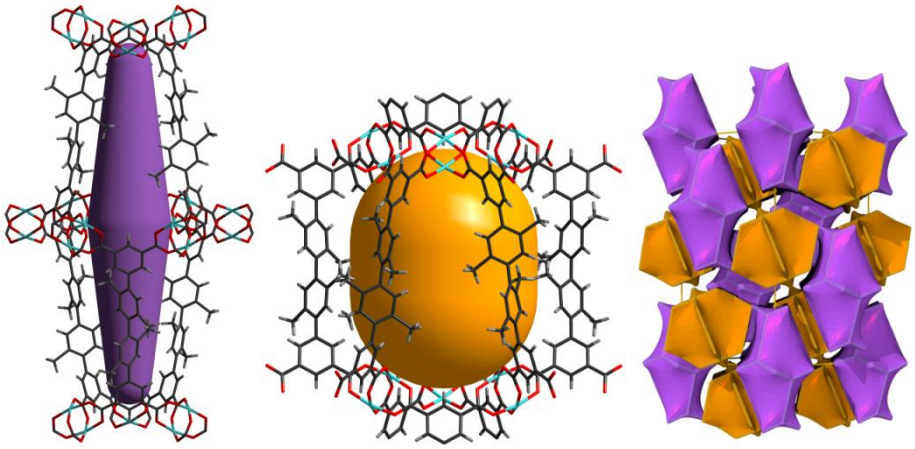

(a) (b) (c)

Figure 2. Views of the single crystal X-ray structure of MFM-130 comprising two type of cages: (a) ellipsoid-shaped cage A of length 33 Å comprising six $(\mathbf{L}^{\mathbf{IV}})^{4-}$ units and 12 $\{Cu_2(COO)_4\}$ paddlewheels; (b) cylindrical cage B (13 Å × 16 Å) formed by 12 linkers and six $\{Cu_2\}$ paddlewheels. (c) View of **fof**-type network and the natural tiling of the two types of cages in the framework.

MFM-131 has the same **fof** topology as MFM-130 with the Kagomé nets pillared by three consecutive paraxylene units from $(\mathbf{L}^{\mathbf{V}})^{4-}$ (Figure 3). Significantly, MFM-131 is non-interpenetrating despite the extra-long strut $(\mathbf{L}^{\mathbf{V}})^{4-}$ used, and this is a rare example of a **fof** framework with large internal voids (63%) employing such an extra-long organic linker. Cage A in MFM-131 is significantly elongated to 4.2 nm in length compared to MFM-130 (3.3 nm) due to the presence of an additional paraxylene unit in the tetracarboxylate strut. With a dense population of methyl groups on the walls of the cage, the diameters of the two ends of the ellipsoid are narrowed to 5 Å compared to the oligophenyl analogue NOTT-104. Cage B in MFM-131 is an elongated nano-sized cylinder of 1.3 × 2.0 nm (1.3 x 1.6 nm for MFM-130). The structural analogue NOTT-104[3b] constructed from a linear tetracarboxylate linker incorporates the same length of strut used in MFM-131, but without the methyl groups. In this case, two identical **fof**-type lattices interpenetrate to form a doubly interpenetrated network in NOTT-104 (Figure 3c). The $\{Cu(isophthalate)\}_n$ Kagomé lattice in NOTT-104 has two types of windows: a smaller triangular window $\{(Cu_2)_3(isophthalate)_3\}$ of 6 Å diameter and a larger hexagonal window $\{(Cu_2)_6(isophthalate)_6\}$ with an opening of 18 Å. Therefore, the narrow end of the elliptical cage from one framework can cross through the wider central opening of a second network, thus allowing network interpenetration in NOTT-104. The π–π interaction between the phenylene units from two different networks further facilitates and stabilises the network interpenetration. In

MFM-131, the opening of the hexagonal window in the Kagomé lattice is significantly smaller because of the presence of six paraxylene units around the window and π–π interactions between the paraxylene units are inhibited, thus successfully preventing interpenetration of the two **fof** lattices.

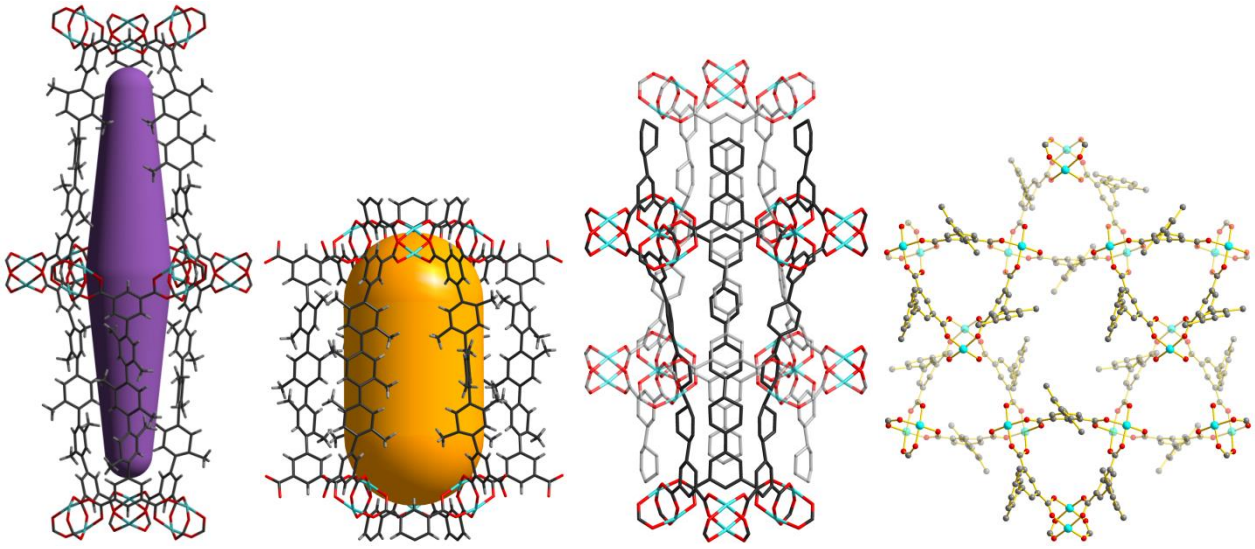

(a) (b) (c) (d)

Figure 3. Views of the single crystal X-ray structure of non-interpenetrated MFM-131. (a) Cage A of 4.2 nm in length; (b) Cage B with dimension of 1.3 nm × 2.0 nm. (c) View of the interpenetrating network in NOTT-104. (d) View of the triangular window in the Kagomé lattice in the MFM-131 framework. The paraxylene rings adjacent to the triangular windows block the space and do not allow two independent networks to interpenetrate.

Stabilities of MFM-130 and MFM-131 and Mechanical Property Calculations. The activation of as-synthesised MFM-130 and MFM-131 were investigated for subsequent gas adsorption studies. Both materials were exchanged with acetone for 24 h before being dried under vacuum at 110 °C to afford the desolvated samples MFM-130a and MFM-131a, respectively. MFM-130a maintained crystallinity after the thermal treatment under vacuum as confirmed by the PXRD analysis (Figure S2). However, MFM-131 after the desolvation process (using both thermal treatment and supercritical CO_2 drying) showed almost complete loss of crystallinity, indicating an inherent instability upon desolvation. In order to understand and rationalize the reasons behind the distinct behaviors of MFM-130 and MFM-131 upon desolvation, we calculated the mechanical properties of both structures in the elastic regime (see Supporting Information).[16,17] The second-order elastic stiffness tensors are shown in Figures ~~S4~~ S7 and S8~~S5~~, and a summary of their average and directional elastic properties are presented in Table 1. It can be observed that both structures have relatively similar mechanical features (due to their isostructural nature), including a marked anisotropy with stiffer

directions (as defined by high Young's modulus) along or near the *c* axis which is, on average, the principal axis of the organic linkers. Surprisingly, both structures display remarkable negative linear compressibility along the *c* axis (–59.9 TPa^{-1} for MFM-130 and –67.6 TPa^{-1} for MFM-131, respectively), which we attribute to a hinging mechanism in the **fof** topology.[18] This opens perspectives for testing of MFM-130 and MFM-131 materials under pressure, as well as other MOFs of **fof** topology, for anomalous mechanical properties.

The main difference in the mechanical properties of MFM-130 and MFM-131 turns out to be the value of their lowest elastic modulus: the shear modulus (Figure 4). While MFM-131 shows lower average Young's and shear moduli than MFM-130, MFM-131 shows an especially low directional shear modulus of 0.48 GPa compared to 1.73 GPa for MFM-130. This difference is linked to the lower density and higher porosity of MFM-131 and not to any change in mechanism since both minimal shear moduli correspond to the same direction. The very low shear modulus of MFM-131 is, to our knowledge, the lowest ever calculated for a non-flexible MOF. It explains the low resistance of MFM-131 to solvent evacuation, during which shear forces develop inside the crystal and which can, if they exceed the shear modulus in a specific direction, lead to mechanical instability and trigger a structural transition or collapse. This behavior is similar to the instability shown by some experimentally synthesized ZIF structures upon removal of solvents and guest molecules.[19]

Table 1. Summary of the mechanical properties of the structural models of MFM-130 and MFM-131 in the elastic regime.

Elastic property	**MFM-130**	**MFM-131**
Bulk modulus (Hill average) (GPa)	11.41	8.77
Young's modulus (Hill average) (GPa)	7.79	4.69
Shear modulus (Hill average) (GPa)	2.81	1.66
Minimal Young's modulus (GPa)	4.43	1.42
Maximal Young's modulus (GPa)	11.25	12.84
Minimal shear modulus (GPa)	1.73	0.48
Maximal shear modulus (GPa)	4.25	2.52
Largest negative linear compressibility (TPa^{-1})	–59.9	–67.6
Largest positive linear compressibility (TPa^{-1})	96.7	136.9

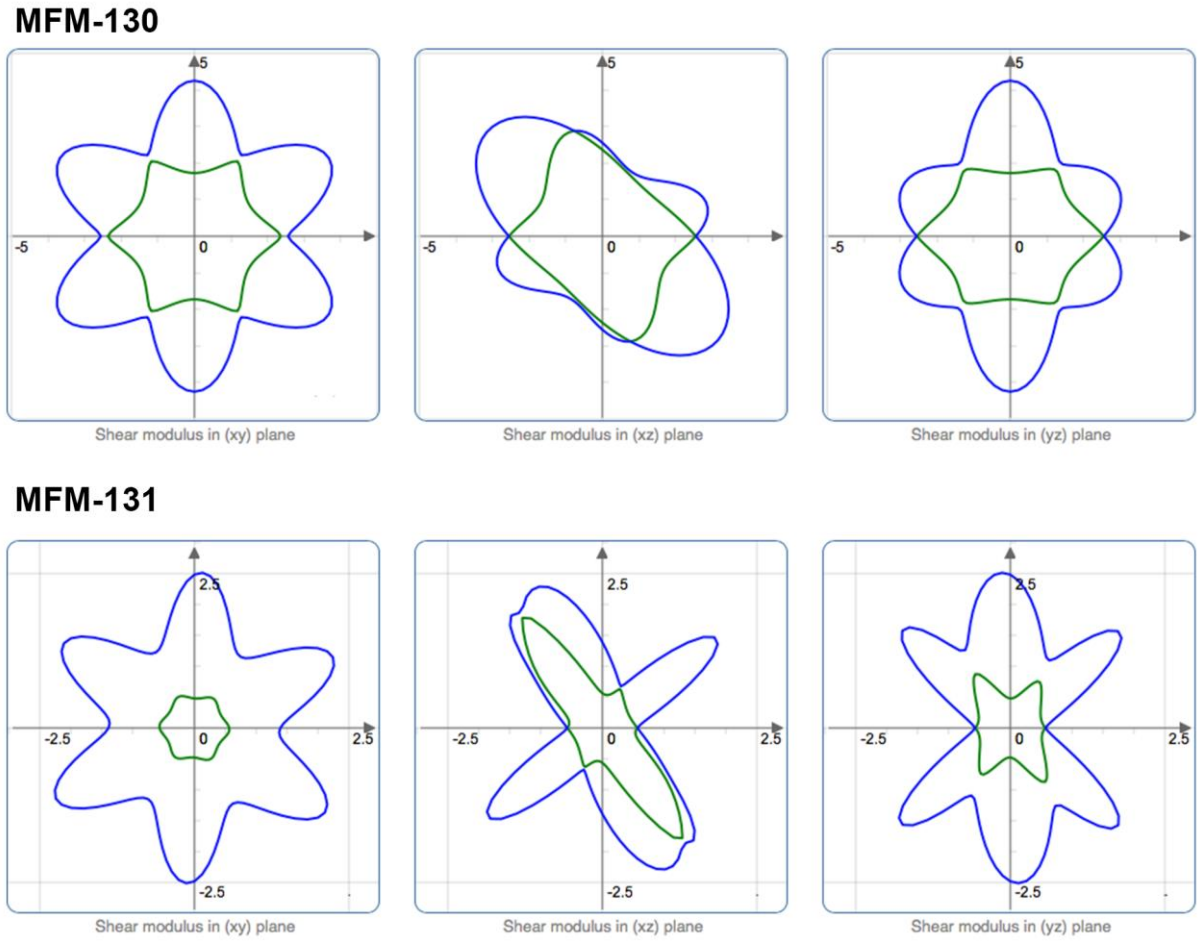

Figure 4. Directional shear modulus of MFM-130 and MFM-131 in the *(xy), (xz) and (yz)* planes. Minimal and maximal values of shear modulus for each direction are plotted in green and blue, respectively.

Porosity of MFM-130a. The total accessible volume in MFM-130a after removal of guest solvates and coordinated water molecules is 60% as determined by the PLATON/VOID routine,[15] and the desolvated framework has a calculated density of 0.642 g/cm^3, which is ~~more dense~~denser than NOTT-102a (0.587 g/cm^3) reflecting the presence of methyl functionalities in the former. The N_2 isotherm for MFM-130a at 77 K shows typical Type I characteristics, indicative of the microporous nature of MFM-130a (Figure 5). The BET surface area is 2173 m^2/g and total pore volume is 1.0 cm^3/g derived from the N_2 isotherm. Due to the multiple methyl substituents occupying additional space, MFM-130a shows both a lower BET surface area and total pore volume than the isostructural frameworks NOTT-102,[3b] NOTT-110[3c] and NOTT-111[3c] containing biphenyl, phenanthrene and hydrophenanthrene subunits, respectively, in the backbones of the tetracarboxylate linkers. The pore diameters in MFM-130a based on the nonlocal density functional theory (NLDFT) model are narrowly distributed between 11–15 Å.

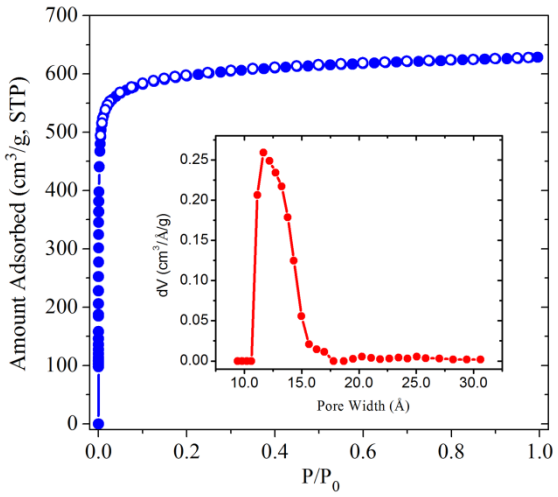

Figure 5. N_2 isotherm for MFM-130a at 77 K. The inset shows the pore size distribution, indicating that the pore diameters are distributed between 11−15 Å according to ~~non-local density functional theoretical~~the NLDFT model.

H_2, CH_4 and CO_2 Sorption Properties of MFM-130a. Cu(II)-based MOFs have been intensively investigated for their H_2 storage properties because of their high surface area and the availability of open Cu(II) sites for providing strong H_2 binding sites.[20,21] Gravimetric H_2 sorption isotherms for MFM-130a were collected at 77 and 88 K up to 20 bar (Figure 6). MFM-130a has a lower surface area compared to non-functionalised NOTT-102 leading to a lower H_2 adsorption capacity of 5.3 wt% at 20 bar and 77 K (6.07 wt% for NOTT-102), consistent with the physical sorption nature of these materials. MFM-130a can adsorb 2.2 wt% of H_2 at 77 K and 1 bar, higher than most other MOFs without open metal sites.[1e,22] The isosteric heat of adsorption for H_2 in MFM-130a was calculated to be 6.6 kJ/mol at zero coverage using the Virial method, higher than those for NOTT-102a, NOTT-110a and NOTT-111a, confirming that the methyl groups in MFM-130a can increase the overlapping potential for H_2 molecules.

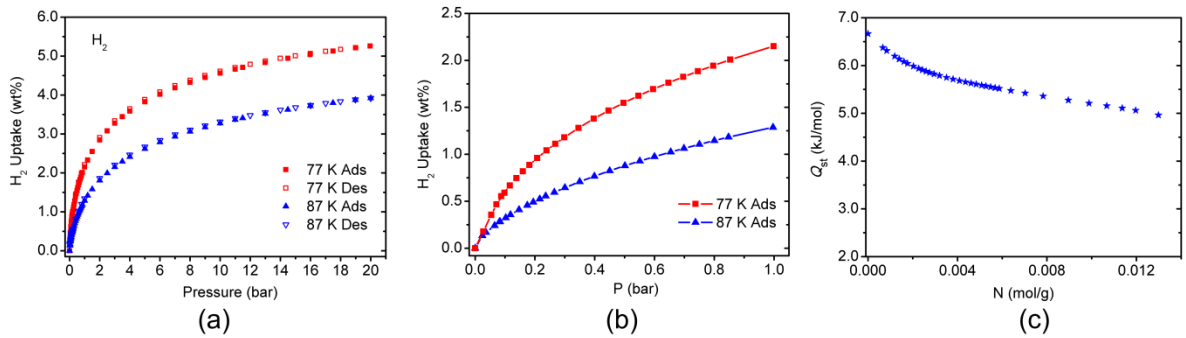

Figure 6. H_2 isotherms for MFM-130a at 77 and 87 K (a) up to 20 bar and (b) up to 1 bar. (c) The isosteric heat of H_2 adsorption as a function of loading for MFM-130a.

CH_4 storage has been widely studied due to the importance of natural gas as a promising alternative to petroleum-based fuels for mobile applications.[23] The CH_4 adsorption isotherms for MFM-130a have been measured at 298 and 273 K up to 20 bar using the same gravimetric method as for the H_2 measurements (Figure ~~S3~~S6). MFM-130a can adsorb a total of 6.9 mmol/g (154 cm^3 (STP)/g) of CH_4 at 298 K and 20 bar, which is moderate compared to other Cu(II)-based MOF materials with high CH_4 capacities (Table 2).[23] At 273 K, the total CH_4 adsorption capacity reaches 9.0 mmol/g (203 cm^3 (STP)/g) at 20 bar. High-pressure CH_4 adsorption data up to 65 bar at 298 K were also collected using volumetric method and the results match well with the gravimetric measurements in the range of 0–20 bar (Figure 7). The excess CH_4 uptake increases with pressure and then reaches the maximum value of 222 cm^3 (STP)/g (equivalent to 143 cm^3 (STP)/cm^3) at 47 bar. The total CH_4 uptake, calculated using the crystal and skeletal densities of the material, reaches a value of 274 cm^3 (STP)/g at 65 bar, corresponding to volumetric uptake of 176 cm^3 (STP)/cm^3. At 35 bar and 298 K, although MFM-130a shows lower gravimetric CH_4 uptake (excess: 219 cm^3 (STP)/g; total: 254 cm^3 (STP)/g) than highly porous MOFs such as NOTT-119[6e] and NU-111,[24] it exhibits higher volumetric CH_4 capacity (excess: 141 cm^3 (STP)/cm^3; total: 163 cm^3 (STP)/cm^3, Table 2). The deliverable CH_4 capacity is also an important factor when considering a material for practical on-board CH_4 storage applications. The deliverable amount of CH_4 in MFM-130a, defined as the difference in uptake between 65 and 5 bar, is 131 cm^3/cm^3. To gain further insight into the nature of framework–CH_4 interactions, the isosteric heats of adsorption (Q_{st}) were calculated from isotherms collected at different temperatures. The Q_{st} for CH_4 is 16.0 kJ/mol at zero surface coverage and, importantly, remains almost constant with increased loading. At loadings higher than 5.0 mmol/g, Q_{st} starts to increase slowly due to the CH_4–CH_4 interactions, which may play an important role at high loadings.

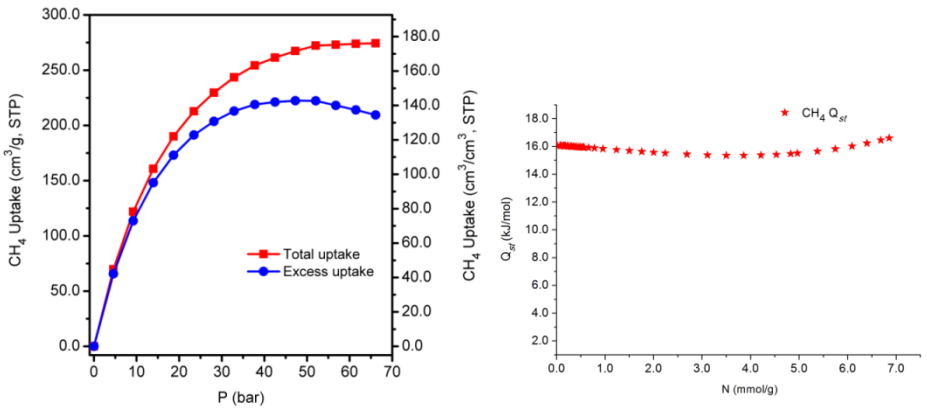

(a) (b)

Figure 7. (a) CH_4 sorption in MFM-130a in the pressure range of 0–70 bar. (b) Variation of heat of adsorption for CH_4 in MFM-130a.

Table 2. Comparisons of CH_4 adsorption data for a variety of MOFs at 298 K.

Material	BET surface area (m^2/g)[a]	Pore Volume (cm^3/g)[a]	Crystal density (g/cm^3)	Total CH_4 uptake at 20 bar		Uptake at 35 bar				Total CH_4 uptake at 65 bar		Deliverable CH_4 amount (65 to 5 bar)	
				cm^3 (STP)/g	v/v	Excess		Total		cm^3 (STP)/g	v/v	cm^3 (STP)/g	v/v
						cm^3 (STP)/g	v/v	cm^3 (STP)/g	v/v				
MFM-130a	2173	1.0	0.642	154	99	219	141	254	163	274	176	204	131
HKUST-1[23a]	1850	0.78	0.883	207	183	231	204	257	227	300	264	215	190
NOTT-100a[23b]	1661	0.68	0.927	181	168	187	173	210	195	249	231	149	138
NOTT-101a[23b]	2805	1.08	0.684	217	148	250	171	284	194	349	239	265	181
NOTT-102a[23b]	3342	1.27	0.587	220	129	266	156	308	181	403	237	324	190
UTSA-76a[3d]	2820	1.09	0.699	234	164	263	184	302	211	367	257	281	196
NOTT-122a[6f]	3286	1.41	0.589	225	133	268[b]	155[b]	314[b]	182[b]	401[b]	232[b]	317[b]	183[b]
NOTT-119a[6e]	4118	2.35	0.361	196	71	215	78	296	107	423	153	370	134
NU-111[23a]	4930	2.09	0.409	220	90	267	109	337	138	504	206	437	179

[a] Measured by N_2 isotherms at 77 K. [b] These data were taken from ref. 23a.

The CO_2 and N_2 adsorption isotherms for MFM-130a were also measured in the pressure range of 0–1 bar at 298 and 273 K (Figure 8). The CO_2 adsorption capacities for MFM-130a at 1 bar are 109 cm^3/g (21.3 wt%) and 59 cm^3/g (11.6 wt%) at 273 and 298 K, respectively. Although these values are lower than those for other highly porous Cu(II)-based MOF materials such as ~~MFM~~NOTT-122[6f] (39.7 wt% at 273 K; 20.4 wt% at 298 K) and ~~MFM~~NOTT-125[25] (40.0 wt% at 273 K; 18.2 wt% at 298 K), which is attributed to the smaller pore size and the absence of CO_2-favourable organic functionalities in MFM-130a, they are higher than most other frameworks without open metal sites such as ZIFs under the same conditions.[26] The heats of adsorption for CO_2 were calculated based on the isotherms at different temperatures by using the Virial method. MFM-130a shows a high heat of CO_2 adsorption of 26 kJ/mol at zero surface coverage, reflecting a strong framework–CO_2 interaction due to the synergistic effects from the narrowed pores caused by the occupation of methyl groups and open Cu(II) sites. Compared to the CO_2 adsorption, MFM-130a shows limited N_2 and CH_4 uptakes at 1 bar and room temperature. The CO_2/N_2 adsorption selectivity values for MFM-130a are 29.2:1 at 298 K and 38.2:1 at 273 K, by evaluating the ratios of Henry's Law constants from single component isotherms. The CO_2/N_2 selectivity for MFM-130a is significantly higher than those for ~~MFM~~NOTT-122a (14.3:1) and ~~MFM~~NOTT-125a (16:1) at 298 K. This is because the methyl groups from the paraxylene units in MFM-130a efficiently reduce the accessible pore size, thus creating enhanced overlapping potential for CO_2 molecules, but at the same time, lowering the adsorption of N_2. Also, MFM-130a shows respectable CO_2/CH_4 selectivity of 9.4 at 273 K and 7.1 at 298 K.

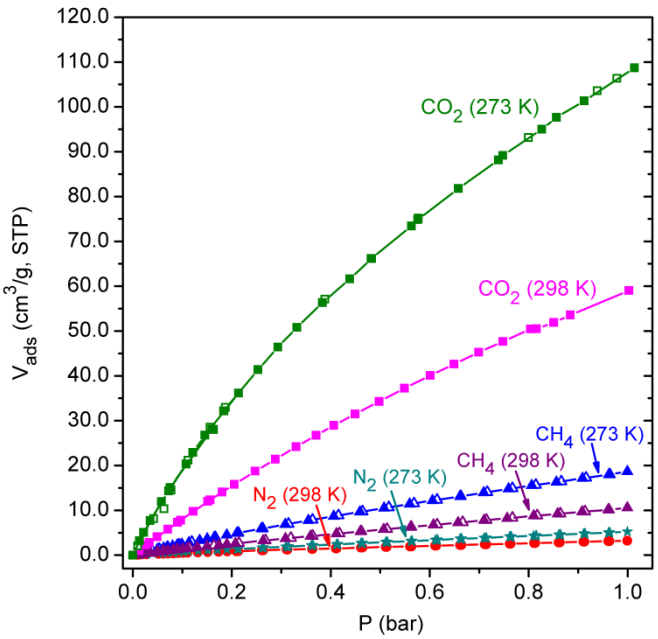

Figure 8. CO_2, CH_4 and N_2 adsorption isotherms for MFM-130a at 298 and 273 K up to 1 bar.

Hydrocarbon Adsorption and Selevtivies in MFM-130a. Light hydrocarbons (C_1–C_3) are important raw chemicals for various industrial applications, and the separation of the pure components from mixtures involves energy-intensive cryogenic distillation processes.[27] In particular, separation of C_2 hydrocarbons from CH_4 is an important industrial process for purification of CH_4, and adsorptive separation has provided an efficient and energy-economic way for these separation tasks.[28] Several MOFs have been realised for their potential excellent selectivities of C_2 hydrocarbons over CH_4 due to the fine control of pore size/shape and the presence of strong ~~C_2s~~ C_2 hydrocarbons binding sites in the MOF structures.[29] Although MOFs with pore sizes comparable to the kinetic diameters (3.3 – 4.4 Å) of C_2 hydrocarbons show enhanced C_2/C_1 selectivities,[29b,29c] they typically suffer from low separation capacities. Therefore, the idealised MOFs for this separation purpose should be the ones showing optimised pore sizes and moderately high porosity, and at the same time, high affinities to C_2 hydrocarbons. Accordingly, pure-component C_2H_2, C_2H_4 and C_2H_6 isotherms for MFM-130a were collected at ambient temperatures (Figure 9). MFM-130a shows moderately high C_2H_2 uptakes of 144 cm^3 (STP)/g at 273 K and 85.9 cm^3/g at 298 K and 1 bar. The C_2H_2 capacities of MFM-130a are comparable to other MOFs with open metal sites showing high C_2H_2 uptakes under the same conditions (Table 3). MFM-130a also adsorbs high amounts of C_2H_4 (115.2 cm^3/g at 273 K; 78.7 cm^3/g at 298 K) and C_2H_6 (124.6 cm^3/g, 273 K; 77.1 cm^3/g, 298 K) at 1 bar. Compared to C_2H_2, C_2H_4 and C_2H_6, MFM-130a shows considerably low CH_4 uptake (18.6 cm^3/g, 273 K; 10.6 cm^3/g, 298 K) at 1 bar, indicating its potential for efficient separation of C_2 hydrocarbons from CH_4.

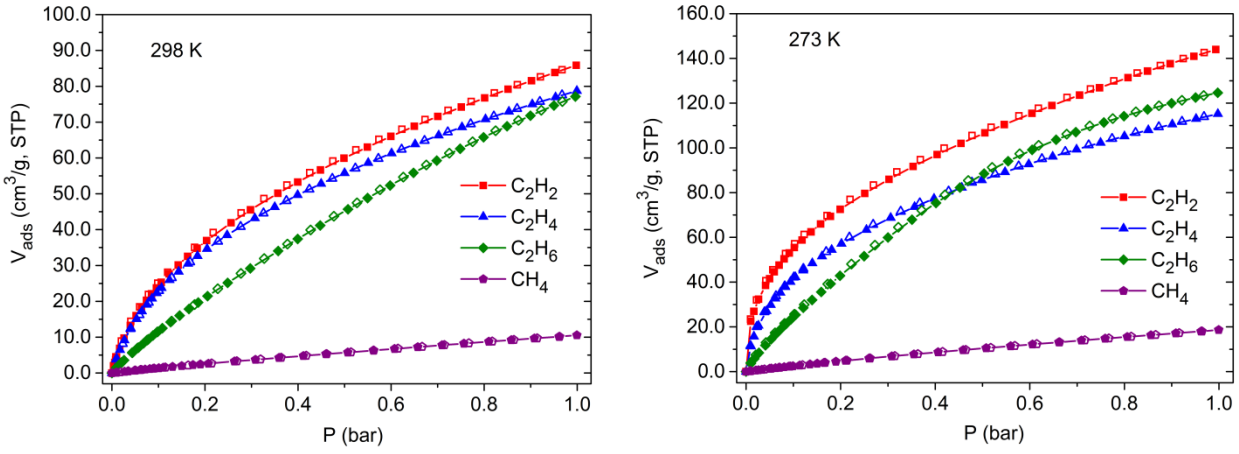

(a) (b)

Figure 9. Adsorption isotherms for hydrocarbons in MFM-130a at (a) 298 K and (b) 273 K in the pressure range of 0–1 bar.

Table 3. C_2H_2 adsorption on various MOFs at 298 K and 1 bar.

Material	BET surface area (m^2/g)	Pore volume[a] (cm^3/g)	D_c[b] (g/cm^3)	C_2H_2 uptake (cm^3 (STP)/g)	Q_{st} for C_2H_2 (kJ/mol)	C_2H_4 uptake (cm^3 (STP)/g)	C_2H_6 uptake (cm^3 (STP)/g)
MFM-130a	2173	1.0	0.642	85.9	33.1	78.7	77.1
$Cu_2(pzdc)_2(pyz)$[c30]	571	-	1.745	42	42.5	-	-
HKUST-1[31a]	1401	0.76	0.879	201	30.4	165.9[d]	137.7[d]
MOF-505[31a]	1139	0.68	0.927	148	25.4	113.4[d]	123.1[d]
NOTT-102a[31b]	3342	1.28	0.587	146	-	128.2	125.9
ZIF-8[31a]	1112	-	0.924	25	13.3	26.7[e]	44.2[e]
ZnMOF-74[32]	747	-	1.231	122	24.0	-	-

[a] The pore volume values were calculated from N_2 isotherms at 77 K. [b] Crystal density calculated from the single-crystal structure for the activated sample. [c] pzdc = pyrazine-2,3-dicarboxylate, pyz = pyrazine. [d] these data were taken from ref. 31b. [e] measured at 301 K.[33]

Virial analyses on the temperature-dependent hydrocarbons adsorption isotherms were performed to evaluate the binding interactions of C_2 hydrocarbons with the framework of MFM-130a and the separation selectivities (Table S2). The isosteric heats of adsorption at zero coverage, calculated based on the Virial parameters, are 33.1, 34.0 and 25.0 kJ/mol for C_2H_2, C_2H_4 and C_2H_6, respectively (ie 16 kJ/mol for CH_4). It is worth noting that the C_2H_2 adsorption enthalpy for MFM-130a at low loading is higher than those for other Cu(II) based MOFs such as MOF-505 (25.4 kJ/mol) and $Cu_3(BTC)_2$ (30.4 kJ/mol),[31a] indicating that the open Cu(II) sites, coupled with the optimised pore diameter induced by the functionalisation of methyl groups in MFM-130a, play important roles in enhancing the binding energy between C_2H_2 and the framework. The selectivities for C_2 hydrocarbons/CH_4 were derived using Henry's Law constants for individual hydrocarbons, based on the equation $S_{ij} = K_H(i)/K_H(CH_4)$. MFM-130a reveals moderate selectivities for C_2H_6 vs CH_4 of 14.4 at 273 K and 10.1 at 298 K. This is consistent with the fact that the interactions of saturated C_2H_6 with the framework is solely based on van der Waals interactions and the selective adsorption of C_2H_6 over CH_4 is mainly based on the size effect of the adsorbates. Importantly, MFM-130a shows high selectivities for C_2H_2 and C_2H_4 over CH_4 of 66.5, 60.0 at 273 K and 34.7, 30.3 at 298 K, respectively. Thus, MFM-130a represents a rare example of a framework material showing simultaneously high C_2 hydrocarbons adsorption capacities and high C_2 hydrocarbons/CH_4 selectivities at ambient temperature.

Conclusions

In summary, we have successfully synthesised two linear tetracarboxylate linkers comprising paraxylene units and the respective $\{Cu_2(COO)_4\}$-based **fof**-type networks MFM-130 and MFM-131. Both these frameworks are non-interpenetrating despite the extra-long organic linkers used and comprise Kagomé lattice layers pillared by the organic oligoparaxylene backbones. In these structures, the paraxylene moieties adjacent to the isothphalate units significantly reduce the accessible openings of windows in the Kagomé lattice layers, thus effectively preventing interpenetration by two networks. This study provides a novel and efficient way for generating non-interpenetrating structures by using paraxylene units as building blocks for organic struts. The mechanical properties calculations of these two MOFs revealed that MFM-131 shows lower average Young's and shear moduli than MFM-130, explaining its instability upon desolvation. Desolvated framework MFM-130a, densely decorated with methyl groups, shows moderately high porosity with BET surface area of 2173 m^2/g and pore volume of 1.0 cm^3/g, with high H_2 uptake capacities at both low and high pressures (2.2 wt% at 1 bar; 5.3 wt% at 20 bar), albeit at low temperature (77 K). The observed increased isosteric adsorption for H_2 in MFM-130a compared to its structural analogues NOTT-102a, NOTT-110a and NOTT-111a clearly indicates that the methyl functionality can enhance the H_2–framework interactions. MFM-130a also shows high volumetric CH_4 adsorption (total 163 cm^3 (STP)/cm^3 at 35 bar) and deliverable (131 cm^3/cm^3 from 65 to 5 bar) capacities at room temperature. Furthermore, the high CO_2 vs N_2, C_2H_2 vs CH_4 and C_2H_4 vs CH_4 selectivities revealed by MFM-130a suggest it to be a promising material for potential carbon capture and natural gas purification applications.

Supporting Information

Crystallographic data for MFM-130 and MFM-131, TGA, PXRD analyses, gas adsorption isotherms and Virial fitting parameters, and theoretical calculations.

Acknowledgements

We thank the EPSRC (U.K. Sustainable Hydrogen Energy Consortium~~, http://www.uk-shec.org.uk/~~) and the University of Nottingham for funding. We are grateful to the EPSRC-funded National Crystallography Service and Diamond Light Source for data collection on Diamond Beamline I19. M. S. gratefully acknowledges receipt of an ERC Advanced Grant and an EPSRC Programme Grant. This research is part

(Project no. 94-938) of the Joint Center of Excellence in Integrated Nano-Systems(JCIN) at King Abdul-Aziz City for Science and Technology (KACST) and Northwestern University (NU). The authors would like to thank both KACST and NU for their continued support of this research. M. J. gratefully acknowledges The Netherlands Organization for Scientific Research (NWO) and the Marie Curie Cofund Action (Rubicon Fellowship). S. G. acknowledges the Swiss National Science Foundation for financial support. F.-X. C. acknowledges the access of HPC resources from GENCI-IDRIS (grant i2014087069).

References

1. (a) Lin, X.; Jia, J.; Hubberstey, P.; Schröder, M.; Champness, N. R. *CrystEngComm* **2007**, *9*, 438−448. (b) Dincă, M.; Long, J. R. *Angew. Chem., Int. Ed.* **2008**, *47*, 6766–6779. (c) Murray, L. J.; Dincă, M.; Long, J. R. *Chem. Soc. Rev.* **2009**, *38*, 1294−1314. (d) Lin, X.; Champness, N. R.; Schröder, M. *Top. Curr. Chem.* **2010**, *293*, 35−76. (e) Suh, M. P.; Park, H. J.; Prasad, T. K.; Lim, D.-W. *Chem. Rev.* **2012**, *112*, 782–835. (f) Sumida, K.; Rogow, D. L.; Mason, J. A.; McDonald, T. M.; Bloch, E. D.; Herm, Z. R.; Bae, T.-H.; Long, J. R. *Chem. Rev.* **2012**, *112*, 724–781. (g) He, Y.; Zhou, W.; Qian, G.; Chen, B. *Chem. Soc. Rev.* **2014**, *43*, 5657–5678.
2. (a) Zhao, D.; Timmons, D. J.; Yuan, D.; Zhou, H.-C. *Acc. Chem. Res.* **2011**, *44*, 123–133. (b) Lu, W.; Wei, Z.; Gu, Z.-Y.; Liu, T.-F.; Park, J.; Park, J.; Tian, J.; Zhang, M.; Zhang, Q.; Gentle III, T.; Bosch, M.; Zhou, H.-C. *Chem. Soc. Rev.* **2014**, *43*, 5561–5593.
3. (a) Lin, X.; Jia, J.; Zhao, X. B.; Thomas, K. M.; Blake, A. J.; Champness, N. R.; Hubberstey, P.; Schröder, M. *Angew. Chem., Int. Ed.* **2006**, *45*, 7358–7364. (b) Lin, X.; Telepeni, I.; Blake, A. J.; Dailly, A.; Brown, C. M.; Simmons, J. M.; Zoppi, M.; Walker, G. S.; Thomas, K. T.; Mays, T. J.; Hubberstey, P.; Champness, N. R.; Schröder, M. *J. Am. Chem. Soc.* **2009**, *131*, 2159–2171. (c) Yang, S.; Lin, X.; Dailly, A.; Blake, A. J.; Champness, N. R.; Hubberstey, P.; Schröder, M. *Chem. Eur. J.* **2009**, *15*, 4829–4835. (d) Li, B.; Wen, H.-M.; Wang, H.; Wu, H.; Tyagi, M.; Yildirim, T.; Zhou, W.; Chen, B. *J. Am. Chem. Soc.* **2014**, *136*, 6207−6210. (e) Kennedy, R. D.; Krungleviciute, V.; Clingerman, D. J.; Mondloch, J. E.; Peng, Y.; Wilmer, C. E.; Sarjeant, A. A.; Snurr, R. Q.; Hupp, J. T.; Yildirim, T.; Farha, O. K.; Mirkin, C. A. *Chem. Mater.* **2013**, *25*, 3539−3543. (f) Wang, X.-S.; Ma, S.; Rauch, K.; Simmons, J. M.; Yuan, D.; Wang, X.; Yildirim, T.; Cole, W. C.; López, J. J.; de Meijere, A.; Zhou, H.-C. *Chem. Mater.* **2008**, *20*, 3145–3152.
4. O'Keeffe, M.; Yaghi, O. M. *Chem. Rev.* **2012**, *112*, 675–702.
5. (a) Furukawa, H.; Ko, N.; Go, Y. B.; Aratani, N.; Choi, S. B.; Choi, E.; Yazaydin, A. O.; Snurr, R. Q.; O'Keeffe, M.; Kim, J.; Yaghi, O. M. *Science*, **2010**, *329*, 424−428. (b) Farha, O. K.; Eryazici, I.; Jeong, N. C.; Hauser, B. G.; Wilmer, C. E.; Sarjeant, A. A.; Snurr, R. Q.; Nguyen, S. B. T.; Yazaydin, A. Ö.; Hupp, J. T. *J. Am. Chem. Soc.* **2012**, *134*, 15016−15021.

6. (a) Nouar, F.; Eubank, J. F.; Bousquet, T.; Wojtas, L.; Zaworotko, M. J.; Eddaoudi, M. *J. Am. Chem. Soc.* **2008**, *130*, 1833−1835. (b) Yan, Y.; Lin, X.; Yang, S.; Blake, A. J.; Dailly, A.; Champness, N. R.; Hubberstey, P.; Schröder, M. *Chem.Commun*. **2009**, 1025−1027. (c) Yan, Y.; Telepeni, I.; Yang, S.; Lin, X.; Kockelmann, W.; Dailly, A.; Blake, A. J.; Lewis W.; Walker, G. S.; Allan, D. R.; Barnett, S. A.; Champness, N. R.; Schröder, M. *J. Am. Chem. Soc*. **2010**, *132*, 4092−4094. (d) Yan, Y.; Blake, A. J.; Lewis, W.; Barnett, S. A.; Dailly, A.; Champness N. R.; Schröder M. *Chem. Eur. J*. **2011**, *17*, 11162−11170. (e) Yan, Y.; Yang, S.; Blake, A. J.; Lewis, W.; Poirier, E.; Barnett, S. A.; Champness, N. R.; Schröder, M. *Chem. Commun*. **2011**, *47*, 9995–9997. (f) Yan, Y.; Suyetin, M.; Bichoutskaia, E.; Blake, A. J.; Allan, D. R.; Barnett, S. A.; Schröder, M. *Chem. Sci*. **2013**, *4*, 1731–1736.
7. (a) Zhang, M.; Chen,Y.-P.; Bosch, M.; Gentle III, T.; Wang, K.; Feng, D.; Wang, Z. U.; Zhou, H.-C.*Angew.Chem.,Int. Ed*. **2014**, *53*, 815–818. (b) Dincă, M.; Dailly, A.; Long, J. R. *Chem. Eur. J*. **2008**, *14*, 10280–10285.
8. (a) Ma, S.; Sun, D.; Ambrogio, M.; Fillinger, J. A.; Parkin, S.; Zhou, H.-C. *J. Am. Chem. Soc*. **2007**, *129*, 1858–1859. (b) Furukawa, H.; Go, Y. B.; Ko, N.; Park, Y. K.; Uribe-Romo, F. J.; Kim, J.; O'Keeffe, M.; Yaghi, O. M. *Inorg. Chem.* **2011**, *50*, 9147–9152.
9. (a) Oisaki, K.; Li, Q.; Furukawa, H.; Czaja, A. U.; Yaghi, O. M. *J. Am. Chem. Soc.* **2010**, *132*, 9262–9264. (b) Farha, O. K.; Malliakas, C. D.; Kanatzidis, M. G.; Hupp, J. T. *J. Am. Chem. Soc.* **2010**, *132*, 950–952.
10. Grunder, S.; Valente, C.;Whalley, A. C.; Sampath, S.; Portmann, J.; Botros, Y. Y.; Stoddart, J. F. *Chem. Eur. J*. **2012**, *18*, 15632–15649.
11. Deng, H.; Grunder, S.; Cordova, K. E.; Valente, C.; Furukawa, H.; Hmadeh, M.; Gándara, F.; Whalley, A. C.; Liu, Z.; Asahina, S.; Kazumori, H.; O'Keeffe, M.; Terasaki, O.; Stoddart, J. F.; Yaghi, O. M. *Science*, **2012**, *336*, 1018–1023.
12. Lörtscher, E.; Elbing, M.; Tschudy, M.; von Hänisch, C.; Weber, H. B.; Mayor, M.; Riel, H. *ChemPhysChem* **2008**, *9*, 2252–2258.
13. (a) Reid, C. R.; Thomas, K. M. *Langmuir* **1999**, *15*, 3206–3218. (b) Reid, C. R.; Thomas, K. M. *J. Phys. Chem. B* **2001**, *105*, 10619–10629.
14. (a) Sheldrick, G. M. *SHELXTL2013: Program for Refinement of Crystal Structures*; University of Göttingen: Göttingen, Germany, 2013. (b) Sheldrick, G. M. *Acta Crystallogr., Sect. A: Found. Crystallogr*. **2008**, *A64*, 112−122.
15. Spek, A. L. *ActaCrystallogr., Sect. D*, **2009**, *65*, 148–155.
16. (a) Ortiz, A. U.; Boutin, A.; Fuchs, A. H.; Coudert, F.-X. *J. Chem. Phys*. **2013**, *138*, 174703. (b) Ortiz, A. U.; Boutin, A.; Fuchs, A. H.; Coudert, F.-X. *Phys. Rev. Lett*. **2012**, *109*, 195502.
17. Tan, J.-C.; Civalleri, B.; Lin, C.-C.; Valenzano, L.; Galvelis, R.; Chen, P.-F.; Bennett, T. D.; Mellot-Draznieks, C.; Zicovich-Wilson, C. M.; Cheetham, A. K. *Phys. Rev. Lett*. **2012**, *108*, 095502.
18. Ogborn, J. M.; Collings, I. E.; Moggach, S. A.; Thompson, A. L.; Goodwin, A. L. *Chem. Sci*. **2012**, *3*, 3011−3017.

19. Bouëssel du Bourg, L.; Ortiz, A. U.; Boutin, A.; Coudert, F.-X. *Systematic Investigation of Thermal and Mechanical Stability of Zeolitic Imidazolate Frameworks (ZIF)*, **2014**, http://arxiv.org/abs/1409.7172
20. Yan, Y.; Yang, S.; Blake, A. J.; Schröder, M. *Acc. Chem. Res.* **2014**, *47*, 296−307.
21. (a) Dincă, M.; Long, J. R. *Angew. Chem., Int. Ed.* **2008**, *47*, 6766–6779. (b) Peterson, V. K.; Liu, Y.; Brown, C. M.; Kepert, C. J. *J. Am. Chem. Soc.* **2006**, *128*, 15578–15579.
22. Rowsell, J. L. C.; Millward, A. R.; Park, K. S.; Yaghi, O. M. *J. Am. Chem. Soc.* **2004**, *126*, 5666–5667.
23. (a) Peng, Y.; Krungleviciute, V.;Eryazici, I.; Hupp, J. T.; Farha, O. K.; Yildirim, T. *J. Am. Chem. Soc.* **2013**, *135*, 11887–11894. (b) He, Y.; Zhou, W.; Yildirim, T.; Chen, B. *Energy Environ. Sci.* **2013**, *6*, 2735–2744.
24. Farha, O. K.; Wilmer, C. E.; Eryazici, I.; Hauser, B. G.; Parilla, P. A.; O'Neill, K.; Sarjeant, A. A.; Nguyen, S. B. T.; Snurr, R. Q.; Hupp, J. T. *J. Am. Chem. Soc.* **2012**, *134*, 9860−9863.
25. Alsmail, N. H.; Suyetin, M.; Yan, Y.; Cabot, R.; Krap, C. P.; Lü, J.; Easun, T. L.; Bichoutskaia, E.; Lewis, W.; Blake, A. J.; Schröder, M. *Chem. Eur. J.* **2014**, *20*, 7317–7324.
26. (a) Banerjee, R.; Furukawa, H.; Britt, D.; Knobler, C.; O'Keefe, M.; Yaghi, O. M. *J. Am. Chem. Soc.* **2009**, *131*, 3875–3877. (b) Morris, W.; Leung, B.; Furukawa, H.; Yaghi, O. K.; He, N.; Hayashi, H.; Houndonougbo, Y.; Asta, M.; Laird, B. B.; Yaghi, O. M. *J. Am. Chem. Soc.* **2010**, *132*, 11006–11008.
27. Eldridge, R. B. *Ind. Eng. Chem. Res.* **1993**, *32*, 2208–2212.
28. (a) Wu, H.; Gong, Q.; Olson, D. H.; Li, J. *Chem. Rev.* **2012**, *112*, 836–868; (b) He, Y.; Zhou, W.; Krishnad, R.; Chen, B. *Chem. Commun.*, **2012**, *48*, 11813–11831.
29. (a) Bloch, E. D.; Queen, W. L.; Krishna, R.; Zadrozny, J. M.; Brown,C. M.; Long, J. R. *Science* **2012**, *335*, 1606–1610. (b) Herm, Z. R.; Bloch, E. D.; Long, J. R. *Chem. Mater.* **2014**, *26*, 323–338. (c) Das, M. C.; Xu, H.; Xiang, S.; Zhang, Z.; Arman, H. D.; Qian, G.; Chen, B. *Chem.–Eur. J.* **2011**, *17*, 7817–7822. (d) Xiang, S. C.; Zhang, Z. J.; Zhao, C. G.; Hong, K.; Zhao, X. B.; Ding, D. R.; Xie, M. H.; Wu, C. D.; Das, M. C.; Gill, R.; Thomas, K. M.; Chen, B. *Nat. Comm.* **2011**, *2*, 204−209.
30. Matsuda, R.; Kitaura, R.; Kitagawa, S.; Kubota, Y.; Belosludov, R. V.; Kobayashi, T. C.; Sakamoto, H.; Chiba, T.; Takata, M.; Kawazoe, Y.; Mita, Y. *Nature* **2005**, *436*, 238–241.
31. (a) Xiang, S.; Zhou, W.; Gallegos, J. M.; Liu, Y.; Chen, B. *J. Am. Chem. Soc.* **2009**, *131*, 12415–12419. (b) He, Y.; Krishna, R.; Chen, B. *Energy Environ. Sci.* **2012**, *5*, 9107–9120.
32. Xiang, S.; Zhou, W.; Zhang, Z.; Green, M. A.; Liu, Y.; Chen, B. *Angew. Chem., Int. Ed.* **2010**, *49*, 4615–4618.
33. He, Y.; Zhang, Z.; Xiang, S.; Wu, H.; Fronczek, F. R.; Zhou, W.; Krishna, R.; O'Keeffe, M.; Chen, B. *Chem. Eur. J.* **2012**, *18*, 1901–1904.

TOC

~~3,5-Dicarboxylate (isophthalate) oligoparaxylenes serve as excellent building units to form porous non-interpenetrating **fof** networks with Cu(II) despite the extra-long organic linker used; gas uptake and selectivities are discussed.~~

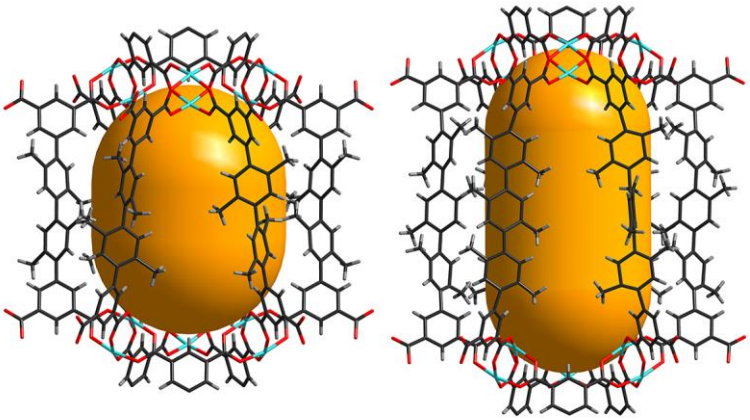

MFM-130 MFM-131